Joint Iterative Image Reconstruction and Field Map Estimation in Low Field MRI

M.L. de Leeuw den Bouter[1], K. Koolstra[2], T.P.A. O'Reilly[2], P. Börnert[2-3], A. Webb[2], R.F. Remis[4] and M.B. van Gijzen[1]

[1]Delft Institute of Applied Mathematics, Delft University of Technology, Delft, The Netherlands
[2]C.J. Gorter Center for High Field MRI, Leiden University Medical Center, Leiden, The Netherlands
[3]Philips Research Hamburg, Hamburg, Germany
[4]Circuits and Systems, Delft University of Technology, Delft, The Netherlands

Introduction

The design of low field portable MRI scanners is of great interest due to its potential clinical relevance in developing countries. Many of the systems have a highly inhomogeneous magnetic field, which can actually be used for spatial encoding and image formation (1–3). However, small inaccuracies in the field map, which can arise from temperature-induced changes or measurement errors, lead to image distortions. Therefore, an accurate field map is needed for each scan, but practically one cannot measure the field map for each scan. Here we propose an algorithm to estimate the field map in an iterative reconstruction, based on a general class of non-linear iterative least-squares estimation methods used, for example, in water/fat separation MRI (4).

Methods

Experimental setup: A Halbach magnet was constructed, containing four rings each with 24 2.5×2.5×2.5cm^3 cubes of N-52 neodymium boron iron (producing a 0.06T magnetic field at the center), with an internal ring of smaller magnets to produce a linear field gradient. The magnetic field was measured on a 5×7.5mm^2 grid using a gaussmeter (Alphalab GM-2).

Simulation: A solenoid coil was modeled for RF transmission/reception. The sample was rotated 36 times with angular increments of $\theta = 10°$. For each rotation, a spin-echo sequence was simulated with RF pulse durations of 20µs, and TE=5 ms; 512 data points; dwell time 2µs. A signal model

$$\mathbf{S}_\theta = ETCR_\theta \mathbf{m} \qquad (1)$$

was used with $\mathbf{m}$ the unknown image (simulated as a Shepp Logan MATLAB phantom), $\mathbf{S_\theta}$ the measured time-domain signal for rotation angle θ, R_θ the corresponding rotation matrix, C a diagonal matrix with uniform spatial coil sensitivity weighted by the coil frequency profile (Q-factor of 13.8 based on an S_{11} measurement) on the diagonal, T a diagonal matrix including the pulse profile (simulated via the Bloch equations) and transmit bandwidth, E the signal encoding matrix with elements $E_{pq} = e^{-2\pi i B_q t_p}$, and B_q the field difference (with respect to the transmitter frequency) in Hz in pixel q. White Gaussian noise was added to the signals such that the SNR was 10.

Image reconstruction: The image is reconstructed by solving the problem

$$\hat{\mathbf{m}} = \min_{\mathbf{m}} \frac{\mu}{2} \left\| \sum_\theta (\mathbf{S}_\theta - ETCR_\theta \mathbf{m}) \right\|_2^2 + \frac{\lambda}{2} TV(\mathbf{m}) \qquad (2)$$

where TV is a total variation operator and μ and λ regularization parameters. Substitution of the perturbations $\mathbf{m}^R = \mathbf{m}^R + \Delta\mathbf{m}^R, \mathbf{m}^I = \mathbf{m}^I + \Delta\mathbf{m}^I$ and $\mathbf{B} = \mathbf{B} + \Delta\mathbf{B}$ in Eq. (1) gives a system for the error terms:

$$\sum_\theta A_\theta^H \begin{bmatrix} \mathbf{S}_\theta^R - \mathbf{a_1} \\ \mathbf{S}_\theta^I - \mathbf{a_2} \end{bmatrix} = \sum_\theta A_\theta^H A_\theta \begin{bmatrix} \Delta\mathbf{m}^R \\ \Delta\mathbf{m}^I \\ \Delta\mathbf{B} \end{bmatrix}. \qquad (3)$$

$\mathbf{S}_\theta^R/\mathbf{S}_\theta^I$ are the real/imaginary parts of the time-domain signal at rotation angle θ. A_θ describes the linearized data model for the error terms and $\mathbf{a_1}/\mathbf{a_2}$ the simulated time-domain signal based on the estimated image $\mathbf{m}$. The final image is reconstructed by the algorithm shown in Figure 1.

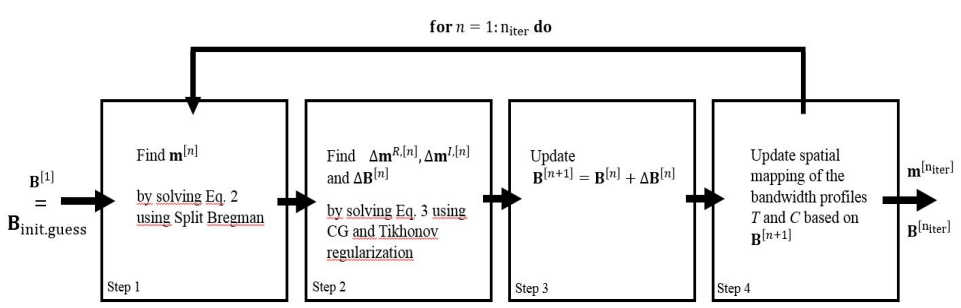

Figure 1. Image reconstruction and field estimation algorithm. In step 1 an estimate of the image is found by solving problem (2) using Split Bregman. 6 outer iterations and 1 inner iteration were used for each iteration of the proposed scheme. Error estimates are found in step 2 by solving Eq. (3) using CG and Tikhonov regularization in which the finite difference regularization matrix enforces smoothness of the field error terms. Finally, the field map is updated using the estimates of the error terms and the transmit and receive maps are updated accordingly.

Results

Figure 2 shows the magnet, the measured field map, the frequency profile of the Tx/Rx coil, and the weighting introduced by the pulse shape. The simulated phantom is shown in Figure 3 discretized at 5mm resolution together with the reconstructed image using the measured field as the encoding function. Figure 4 shows how the image quality degrades if the field map is shifted by (a) 200Hz and (d) 1500Hz for each pixel in the reconstruction, corresponding to small uniform magnet/system temperature changes of 0.1°C and 0.5°C, respectively. Figures 4b,e show the reconstructed images after 25 iterations of the proposed scheme. The relative errors of the field and the image decrease with the number of iterations, as shown in Figures 4c,f. Figures 4g-i show results for a spatially random error in the field of between -1000 and +1000Hz.

Discussion

Simulation results showed that distortions in the field map can be corrected by simultaneously estimating the field map and image in the reconstruction process. The quality of the reconstructed images after 25 iterations is comparable to that of the images reconstructed with the true field map. For very large field distortions a second-order error model could improve the reconstruction. The field inhomogeneity spatially encodes the time-domain signals, but the encoding power is relatively weak, resulting in an ill-posed minimization problem: further magnet optimization could increase the reconstruction performance in these low-encoding regions. Future work should investigate whether this algorithm can be extended to correct for continuous field drifts during the measurement.

Conclusion

The joint field map estimation and image reconstruction algorithm is able to improve the image quality in low field MRI in the presence of uncertainties in the field map.

Acknowledgements

M.L. de Leeuw den Bouter is funded by NWO-WOTRO Grant W07.303.101. K. Koolstra is funded by the European Research Council Advanced Grant 670629 NOMA MRI.

References

1. Cooley C, Stockmann J, Armstrong B, et al. 2D Imaging in a Lightweight Portable MRI Scanner Without Gradient Coils. Magnetic Resonance in Medicine. 2015;72(3):1–15.
2. Ren ZH, Obruchkov S, Lu DW, et al. A low-field portable magnetic resonance imaging system for head imaging. Progress in Electromagnetics Research Symposium. 2017;2017–Novem(c):3042–3044.
3. Zimmerman Cooley C, Haskell MW, Cauley SF, et al. Design of Sparse Halbach Magnet Arrays for Portable MRI Using a Genetic Algorithm. IEEE Transactions on Magnetics. 2017;54(1):1–12.
4. Reeder SB, Wen Z, Yu H, et al. Multicoil Dixon Chemical Species Separation with an Iterative Least-Squares Estimation Method. Magnetic Resonance in Medicine. 2004;51(1):35-45.

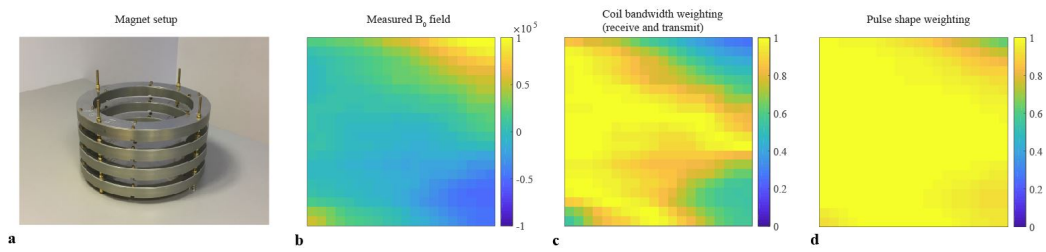

Figure 2. (a) Photograph of four ring Halbach magnet. (b) Difference field map in Hz (with respect to the transmitter frequency) measured with a Hall probe with a resolution of 5×7.5mm2 within a 10×10cm2 FOV, and rescaled to the desired reconstruction resolution using interpolation. (c) The bandwidth of the transmit/receive coil (Q-factor of 13.8) was normalized and spatially mapped to the measured field map. (d) The effect of the pulse shape and length on the flip angle distribution was taken into account by spatially mapping the normalized frequency profile of the pulse to the measured field map.

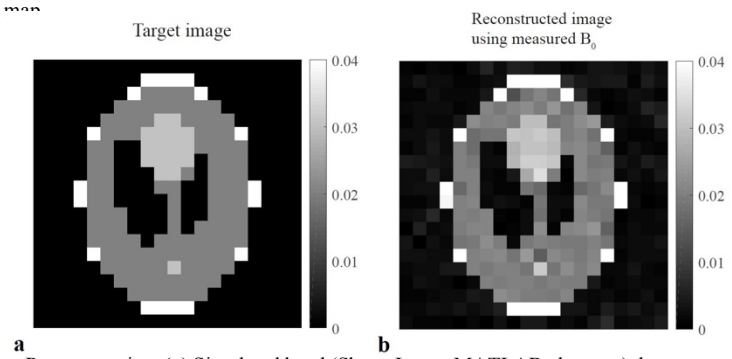

Figure 3. Image Reconstruction. **(a)** Simulated head (Shepp Logan MATLAB phantom) that was used to generate time-domain signals with an SNR of 10, using the measured field map in the signal model. **(b)** An image was reconstructed from these signals using the Split Bregman algorithm with total variation regularization. The desired resolution of 5 mm is obtained with a 20×20 reconstruction matrix. Regularization parameters were empirically defined and set to $\boldsymbol{\mu = 2 \cdot 10^{-4}}$, $\boldsymbol{\lambda = 200}$.

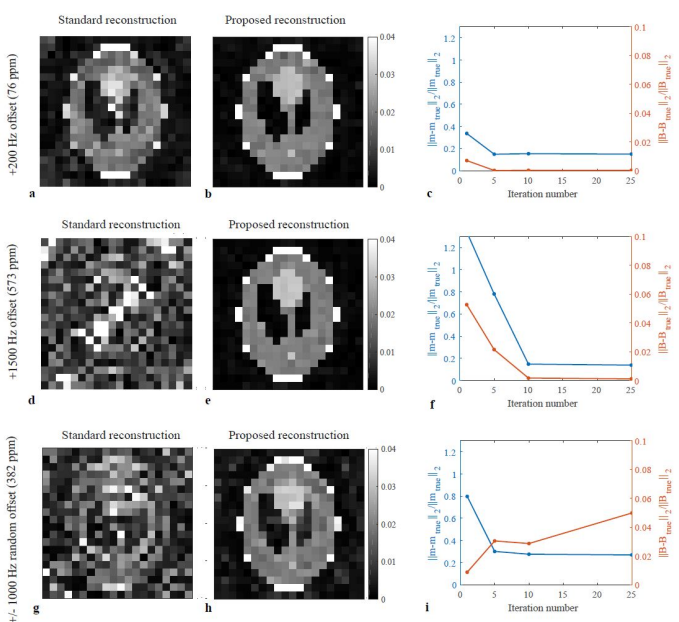

Figure 4. Joint image reconstruction and field map estimation. The quality of the image degrades when the field map contains a frequency shift of **(a)** 200Hz (76ppm) and **(d)** 1500Hz (573ppm) for each pixel, and random measurement errors between **(g)** -1000 and +1000Hz (±382ppm). **(b,e,h)** After 25 iterations of the joint reconstruction scheme the quality is much closer to that of the target image in Figure 1a. Small errors are still present in **(h)**, for which the smoothness assumption of the field error does not hold. **(c,f,i)** The relative error in the main field decreases with the iteration number.